Diagnosis of Wing Icing Through Lift and Drag Coefficient Change Detection for Small Unmanned Aircraft ⋆

Kim Lynge Sørensen * **Mogens Blanke** *,** **Tor Arne Johansen** *

* *Autonomous Marine Operations and Systems, Department of Engineering Cybernetics, the Norwegian University of Science and Technology, O. S. Bragstads Plass 2D, NO-7491 Trondheim, Norway (e-mail: kim.sorensen@itk.ntnu.no, mogens.blanke@itk.ntnu.no, tor.arne.johansen@itk.ntnu.no).*
** *Department of Electrical Engineering, Technical University of Denmark, DK-2800 Kgs. Lyngby, Denmark (e-mail: mb@elektro.dtu.dk)*

Abstract: This paper address the issue of structural change, caused by ice accretion, on UAVs by utilising a Neyman Pearson (NP) based statistical change detection approach, for the identification of structural changes of fixed wing UAV airfoils. A structural analysis is performed on the nonlinear aircraft system and residuals are generated, where a generalised likelihood ratio test is applied to detect faults. Numerical simulations demonstrate a robust detection with adequate balance between false alarm rate and sensitivity.

Keywords: Structural Change Detection; Aircraft Ice accretion; Aircraft Icing Detection; UAV; Fixed-Wing UAV; Statistical Change Detection;

1. INTRODUCTION

Structural changes due to ice accretion are common causes for unmanned aerial vehicle incidents in cold and humid regions. For fixed wing UAVs the leading edge of airfoil surfaces is the primary surface exposed to these changes, causing a significant reduction in aerodynamic ability, i.e. decreasing lift and manoeuvrability, and increasing drag, weight, and consequently power consumption. Timely detection of such changes could potentially prevent icing related UAV incidents.

The use of unmanned aerial vehicles (UAV)s has increased significantly within the last decade, operating in surveillance and reconnaissance primarily. UAVs are very well suited for operating in conditions that are deemed unsafe for humans, Arctic operations being relevant and significant mentioning. Consequently, reliable and efficient UAV operation in harsh environments, as the Arctic, is desirable.

In aviation, icing conditions are atmospheric conditions that can lead to the formation of ice on aircraft. In-flight icing can occur when an aircraft passes through air that contain droplets of water (humid air), and where the temperature at the point of the droplets impact with the aircraft, is 0° C or colder.

The risks of aircraft icing have been known since the early 1900's. The effects of icing depends upon the location, and the type, of the formed ice. Icing can occur on wings, control surfaces, horizontal and vertical stabilizers, fuselage nose, landing gear doors, engine intakes, fuselage air data ports and sensors, and drain system outputs. In this paper focus is on detecting ice forming on the leading edge of a UAV wings.

In the literature there exists numerous approaches to fault detection and isolation (FDI) techniques applied for the detection and isolation of actuator and sensor faults on UAVs, see Bateman et al. (2011), Ducard (2009), and Ducard and Geering (2008) for the former and for the later see Fravolini et al. (2009). Detection of control surface defects was studied in Blanke and Hansen (2013), where fault parameter adaptation and fault diagnosis was attempted simultaneously. For the specific detection problem addressed in this paper, literature is more sparse. In Tousi and Khorasani (2009) and Tousi and Khorasani (2011) icing is diagnosed through an observer-based fault diagnosis technique that detects and estimates the percentage of ice present on the aircraft wing, relying on a linearised lateral model of the aircraft. In Cristafaro et al. (2015) a multiple models adaptive estimation framework is proposed and in Cristafaro and Johansen (2015) an input observer framework for designing icing diagnosis filters is developed and validated through a case study.

⋆ This work has been carried out at the Centre for Autonomous Marine Operations and Systems (AMOS), supported by the Research Council of Norway through the Centres of Excellence funding scheme, Project number 223254 - AMOS. The Norwegian Research Council is acknowledged as the main sponsor of AMOS.

This paper addresses the issue of detecting ice when it occurs on the leading edge of small scale UAV wings, in flight, by means of a structural change detection and identification approach using a nonlinear longitudinal model of the aircraft. Under the assumption that model uncertainties, such as unknown aerodynamic coefficients, are a priori estimated, the scheme is based on a structural analysis performed on the system, with residual generation as an outcome. A generalised likelihood ratio test (GLRT) is then utilised to detect any changes in the generated residuals, where any constant change would constitute an occurance of a fault.

The remainder of the paper is organized as follows. In Section 2, background theories and modelling used in the paper are reviewed. Section 3 provides the main contribution of the paper, where the proposed fault diagnosis system for detecting and isolating faults caused by icing on UAVs is presented. A performance assessment is conducted through simulations in Section 4. Finally, the paper is concluded in Section 5.

2. PRELIMINARIES

This section provides background information needed to develop the proposed fault diagnosis solution. First the consequences of icing is described followed by a presentation of the aircraft model used throughout the paper.

2.1 Icing Consequences

In flight icing forming on the leading edge of an aircraft causes a disruption to the airflow around the wings, i.e. a change in the aerodynamic properties of the wing. The consequences are identified as a reduction in lift and controllability, as well as an increase in drag and weight. Most UAVs are equipped with an autopilot. The autopilot will control the aircraft to maintain a certain height above ground, a certain forward airspeed, and a course, as specified by any user. When ice forms on the leading edge of the wings of the aircraft, the autopilot will, in an attempt to maintain the height and speed, increase the angle-of-attack of the aircraft and the thrust of the engine.

2.2 Sensors

Utilisation of the following sensor suite is assumed

- An IMU procures measurements of angular velocities and specific force
- A pitot-static tube providing measurements of the relative velocity in the longitudinal axis of the aircraft
- An engine speed sensor

2.3 Aircraft Model - Kinematics

Let $\mathbf{v}_g^b = (u, v, w)$ denote the decomposition of the ground velocity vector $\mathbf{v}_g$, defined in the Earth-fixed North-East-Down (NED) frame, into the BODY frame, and let p, q, and r be the angular rates. This allows for the aircraft kinematics to be written as

$$\dot{u} - rv + qw = a_x, \tag{1}$$
$$\dot{v} - pw + ru = a_y, \tag{2}$$
$$\dot{w} - qu + pv = a_z, \tag{3}$$

with acceleration components a_x, a_y, and a_z decomposed in the BODY frame. Let the wind velocity vector relative to Earth be denoted $\mathbf{v}_w = (u_w, v_w, w_w)$. The aircraft velocity relative to the wind velocity is then $\mathbf{v}_r = \mathbf{v}_g - \mathbf{v}_w$. Consequently the relative velocity in the BODY frame, denoted $\mathbf{v}_r^b = (u_r, v_r, w_r)$, can be written as

$$\begin{pmatrix} u_r \\ v_r \\ w_r \end{pmatrix} = \begin{pmatrix} u \\ v \\ w \end{pmatrix} - R_n^b \begin{pmatrix} u_w \\ v_w \\ w_w \end{pmatrix}, \tag{4}$$

where R_n^b is the rotation matrix from NED to BODY frame defined by the Euler angles roll (ϕ), pitch (θ), and yaw (ψ)

The relative velocity components u_r, v_r, and w_r are related to the airspeed V_a through

$$u_r = V_a \cos(\alpha)\cos(\beta), \tag{5}$$
$$v_r = V_a \sin(\beta), \tag{6}$$
$$w_r = V_a \sin(\alpha)\cos(\beta), \tag{7}$$
$$V_a = \sqrt{u_r^2 + v_r^2 + w_r^2}, \tag{8}$$

with α and β denotes the angle-of-attack (AOA) and sideslip angle (SSA). For small scale UAVs the AOA and SSA are generally not measured, nor is the wind speed, instead they require estimation. In Long and Song (2009) a sensor fusion approach is applied for just this purpose, where the estimation is based on estimates of velocities and wind speeds, and on the general relations (see Beard and McLain (2012), Long and Song (2009), and Stevens and Lewis (2003))

$$\alpha = \tan^{-1}\left(\frac{w_r}{u_r}\right), \qquad \beta = \sin^{-1}\left(\frac{v_r}{V_a}\right).$$

A similar objective, but different approach, is utilised in Johansen et al. (2015), where wind velocities, AOA, and SSA are estimated through kinematic relationships and a Kalman filter, thereby avoiding the need to know aerodynamic models or other aircraft parameters. Based on either of the aforementioned estimation methods α, β, $\mathbf{v}_w$, and consequently V_a (denoted $\hat{V}_a$) is assumed known.

2.4 Aircraft Model - Forces and Aerodynamics

Let the specific force vector, decomposed in the BODY frame, be (f_x, f_y, f_z), defined as

$$f_x = a_x + g\sin(\theta), \tag{9}$$
$$f_y = a_y - g\sin(\phi)\cos(\theta), \tag{10}$$
$$f_z = a_z - g\cos(\phi)\cos(\theta), \tag{11}$$

where g is the gravitational constant. (f_x, f_y, f_z) is related to the aerodynamic forces and thrust force of the aircraft by

$$f_x = \frac{1}{\mathrm{m}}\left(F_{a_x} + F_t\right), \tag{12}$$
$$f_y = \frac{1}{\mathrm{m}}F_{a_y}, \tag{13}$$
$$f_z = \frac{1}{\mathrm{m}}F_{a_z}, \tag{14}$$

where m is the aircraft mass and F_t denotes the thrust force, which is assumed to be aligned with the longitudinal axis of the aircraft. $\left(F_{a_x}, F_{a_y}, F_{a_z}\right)$ are aerodynamic forces represented as a vector decomposed in the BODY frame.

The thrust developed by the engine, as presented in Beard and McLain (2012), is described by

$$F_t = \frac{1}{2}\rho S_p C_p \left(k_p^2 \omega_p^2 - V_a^2\right), \tag{15}$$

where ρ is the air density, S_p and C_p are propeller coefficients. k_p is a constant that specify the motor efficiency and ω_p denotes the angular velocity of the propeller.

Focus of the fault diagnosis approach presented in this paper is confined to regard longitudinal and vertical change detection. For that purpose the relevant aerodynamic forces can be described by

$$F_{a_x} = \frac{1}{2}\rho V_a^2 S C_X(\alpha), \tag{16}$$

$$F_{a_z} = \frac{1}{2}\rho V_a^2 S C_Z(\alpha), \tag{17}$$

where S is the wing surface area and $\frac{1}{2}\rho V_a^2$ represents the dynamic pressure. C_X and C_Z are composed of lift C_L and drag C_D coefficients and depend on α, as described in Beard and McLain (2012) and Stevens and Lewis (2003), i.e.

$$C_X = C_L(\alpha)\sin(\alpha) - C_D(\alpha)\cos(\alpha), \tag{18}$$

$$C_Z = -C_L(\alpha)\cos(\alpha) - C_D(\alpha)\sin(\alpha). \tag{19}$$

The aerodynamic coefficients, C_X and C_Z, are unknown quantities. In Hansen and Blanke (2013) estimation is achieved using a standard adaptive observer updating approach. However, within the scope of this paper nominal values of these estimates, i.e. no icing, are assumed known. The estimated parameters are denoted $\hat{C}_X$ and $\hat{C}_Z$, respectively.

3. FAULT DIAGNOSIS

The fault diagnosis objective is to detect and isolate the structural fault that occurs when icing forms on the leading edge of aircraft wings. The diagnosis is complicated by model uncertainties, which can be attributed to the non measurable coefficients C_X and C_Z found in the expressions for the longitudinal and lateral aerodynamic forces. The objective is achieved through residual generation and a NP change detection solution. The former is obtained as presented in Blanke et al. (2006) and the latter as presented in Kay (1998).

3.1 Structural Analysis

Given the nonlinear model of the aircraft, described in the previous section, the following constraints (or subsystems) for the structural analysis can be formulated

$$c_1: \quad f_x = \frac{1}{\mathrm{m}}\left(F_{a_x}(\hat{V}_a, \hat{C}_X) + F_T(\hat{V}_a, \omega_p)\right),$$

$$c_2: \quad f_z = \frac{1}{\mathrm{m}} F_{a_z}(\hat{V}_a, \hat{C}_Z),$$

$$m_1: \quad y_1 = f_x, \quad m_2: \quad y_2 = f_z, \quad m_3: \quad y_3 = \omega_p,$$

$$e_1: \quad y_4 = \hat{V}_a, \quad e_2: \quad y_5 = \hat{C}_X, \quad e_3: \quad y_6 = \hat{C}_Z,$$

Note that the constraints denoted e_1, e_2, and e_3 are considered measured parameters.

Residuals are identified using the methods described in Blanke et al. (2006) and confirmed using the Matlab tool SATool presented in Blanke and Lorentzen (2006), as $\{c_1, c_2\}$

$$r_1 = \frac{\rho}{2\mathrm{m}}\left(y_4^2 S y_5 + S_p C_p\left(k_p^2 y_3^2 - y_4^2\right)\right) - y_1, \tag{20}$$

$$r_2 = \frac{\rho}{2\mathrm{m}} y_4^2 S y_6 - y_2, \tag{21}$$

3.2 Simulator

To asses the performance of the proposed icing detection solution, numerical simulations have been conducted utilising Matlab and Simulink, with a sample time of 0.01s. The simulations have been based on the complete, 6-degree of freedom *Zagi* model, of the small unmanned aircraft system presented in Beard and McLain (2012), including the autopilot module. Measurement noise is modelled as zero-mean white Gaussian noise, $\mathcal{N}(0, \sigma_{m,*})$, with standard deviations aligned with the ones found in Langelaan et al. (2011), i.e. $\sigma_{m,u_r} = 0.1$ [m/s] and $\sigma_{m,f_x}, \sigma_{m,f_z} = 0.1$ [m/s^2]. Wind is modelled as a constant wind field with added turbulence, which is generated as white noise filtered through a Dryden gust model, an approach presented by Langelaan et al. (2011) and utilised Beard and McLain (2012). The Dryden transfer functions for the wind turbulence are defined by

$$H_u(s) = \sigma_{D,u}\sqrt{\frac{2V_a}{L_u}} \cdot \frac{1}{s + V_a/L_u}, \tag{22}$$

$$H_v(s) = \sigma_{D,v}\sqrt{\frac{3V_a}{L_v}} \cdot \frac{s + V_a/(\sqrt{3}L_v)}{(s + V_a/L_v)^2}, \tag{23}$$

$$H_w(s) = \sigma_{D_w}\sqrt{\frac{3V_a}{L_w}} \cdot \frac{s + V_a/(\sqrt{3}L_w)}{(s + V_a/L_w)^2}, \tag{24}$$

where σ_{D*} and L_* are the turbulence intensities and spatial wavelength along the vehicle frames, respectively. For the simulations the Dryden model has been implemented with a constant nominal airspeed $V_a = V_{a_0}$. The gust model used is for low altitude, moderate turbulence, with numerical values for the turbulence parameters presented in Table 1

Table 1. Measurement noise levels and Dryden gust parameters

altitude,	50	[m]
L_u, L_v,	200	[m]
L_w,	50	[m]
$\sigma_{D,u}$, $\sigma_{D,v}$,	2.12	[m/s]
$\sigma_{D,w}$,	1.4	[m/s]
V_{a_0},	14	[m/s]

The structural fault, icing on the leading edge of the wing entails, has been imposed upon the aircraft as a 10% increase in the drag coefficient and a 10% decrease in the lift coefficient, which are well within the penalties described in Lynch and Khodadoust (2001). For clarifying purposes Figures 1 and 2 display the responses of the aircraft system to icing. The former show responses in altitude, airspeed, and pitch angle. The latter display autopilot responses, i.e. thrust and elevator displacements. The fault is imposed at $t = 500$s with ice forming over a period lasting 25 seconds.

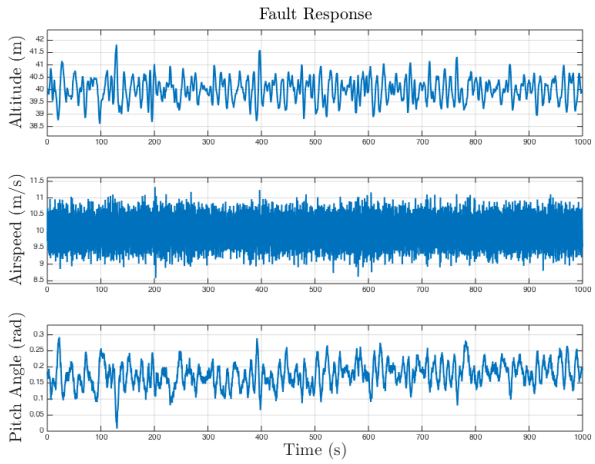

Fig. 1. Response to structural fault- 1. altitude, 2. airspeed, 3. pitch angle.

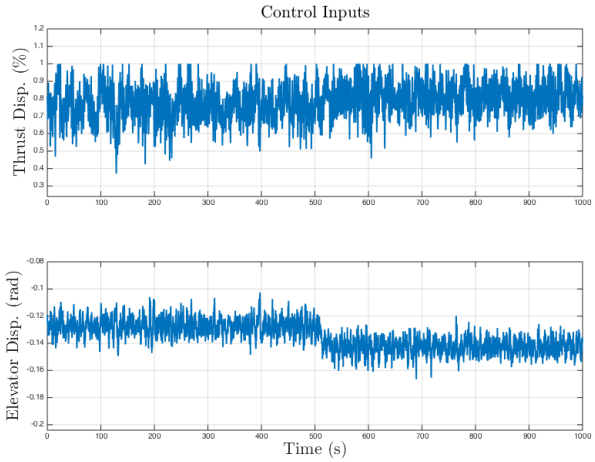

Fig. 2. Autopilot response to structural fault- 1. thrust displacement, 2. elevator displacement.

3.3 Change Detection

Fault detection is in this paper achieved by detecting changes in the residual signals (20) and (21). The proposed detection solution relies on $\hat{C}_X$ and $\hat{C}_Z$ under nominal flight conditions. When $\hat{C}_X$ and $\hat{C}_Z$ display unexpected changes, a bias is introduced into the residuals and a structural fault (icing on the leading edge of the airfoil) is said to have occurred. Note that r_1 and r_2 can be presented as

$$r_1 = \frac{\rho}{2\mathrm{m}} V_a^2 S \left(\hat{C}_X - C_X \right), \tag{25}$$

$$r_2 = \frac{\rho}{2\mathrm{m}} V_a^2 S \left(\hat{C}_Z - C_Z \right), \tag{26}$$

where $\hat{C}_* - C_* \neq 0$ whenever icing is forming on the leading edge of the airfoil.

The response of the two residuals and the distributions for faultless and faulty evolutions, are displayed in Figure 3.

A Generalised Likelihood Ratio Test (GLRT) is used to distinguish between two hypotheses stated about the residual signal. The problem is mathematically expressed

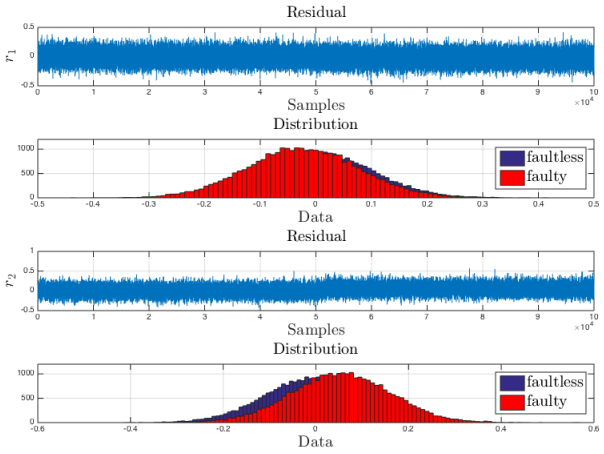

Fig. 3. Residuals r_1 and r_2, with distributions for the faultless and faulty operations.

as the following detection problem.

$$\mathcal{H}_0 : x[n] = w[n] \quad n = 0, 1, \ldots N-1, \tag{27}$$

$$\mathcal{H}_1 : x[n] = A + w[n] \quad n = 0, 1, \ldots N-1, \tag{28}$$

where A is unknown and $w[n]$ is white Gaussian noise with unknown variance σ^2. N is the window size. The $\mathcal{H}_0$ hypothesis describes the case where the signal contain the expected noise only, whereas the alternative hypothesis $\mathcal{H}_1$, other than containing the expected noise, also contain an offset A from zero. If an offset is identified it implies a significant difference between the model and the measurement, hence a fault is concluded to be present. In Figures 4 and 5 the probability plot and autocorrelation of the two relevant residuals are displayed. As seen in the figures the residuals contain uncorrelated samples.

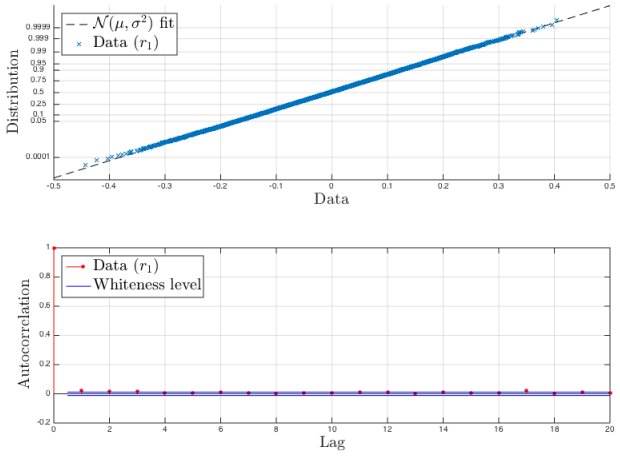

Fig. 4. Residual r_1 data distribution fit and autocorrelation.

The probability plots show that the residuals follows a Gaussian distribution with a general form

$$p(x; \mu, \sigma) = \frac{1}{\sigma\sqrt{2\pi}} e^{-\frac{(x-\mu)^2}{2\sigma^2}}. \tag{29}$$

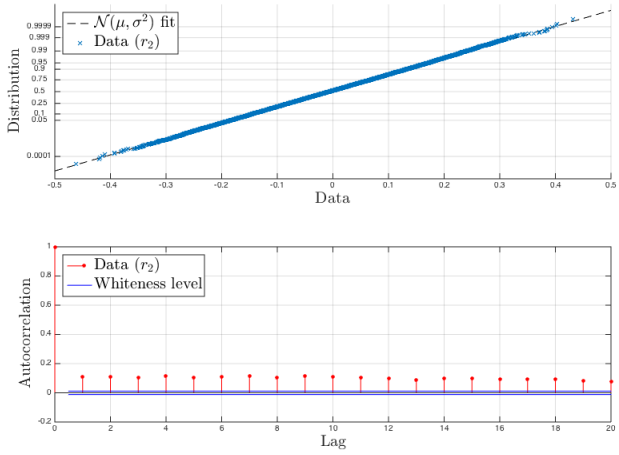

Fig. 5. Residual r_2 data distribution fit and autocorrelation.

The GLRT is based on the likelihood ratio between the probability of the two hypotheses given a window of data. The GLRT decides $\mathcal{H}_1$ if

$$L_G(\mathbf{x}) = \frac{p(\mathbf{x}; \hat{A}, \hat{\sigma}_1^2, \mathcal{H}_1)}{p(\mathbf{x}; \hat{\sigma}_0^2, \mathcal{H}_0)} > \gamma, \tag{30}$$

where $[\hat{A}\ \hat{\sigma}_1^2]^T$ is the maximum likelihood estimate (MLE) of the vector $[A\ \sigma_1^2]$ under $\mathcal{H}_1$ and $\hat{\sigma}_0^2$ is the MLE of σ_0^2 under $\mathcal{H}_0$. The decision function (or threshold) is denoted γ. $\hat{A}$, $\hat{\sigma}_1^2$, and $\hat{\sigma}_0^2$ are determined by maximising (29) with $\mu = A$ and $\mu = A = 0$, respectively. For the MLEs under $\mathcal{H}_1$ this results in

$$\hat{\sigma}_1^2 = \frac{1}{N} \sum_{n=0}^{N-1} (x[n] - \bar{x})^2, \tag{31}$$

with $\bar{x}$ being the sample mean of $x[n]$ and where $\bar{x} = \hat{A}$. For the MLE under $\mathcal{H}_0$ maximising (29), assuming $\mu = A = 0$, leads to

$$\hat{\sigma}_0^2 = \frac{1}{N} \sum_{n=0}^{N-1} x[n]^2. \tag{32}$$

With this the following test statistic can be derived (see Kay (1998))

$$T(\mathbf{x}) = N \ln \left(\frac{\hat{\sigma}_0^2}{\hat{\sigma}_1^2} \right). \tag{33}$$

A theoretical threshold γ is determined according to the Neyman Pearson theorem found in Kay (1998). Given a signal $f(t)$ that behaves according to the probability density function $p(f(t); \mathcal{H}_0)$ under $\mathcal{H}_0$, the threshold that maximises the probability of detection P_D is found from

$$P_{FA} = \int_{\{f: L_G(f) > \gamma\}} p(f; \mathcal{H}_0) \mathrm{d}f, \tag{34}$$

where P_{FA} is the desired probaility of false alarm. For the modified GLRT, here denoted $T(\mathbf{x})$, an asymptotic result exists for large data records ($N \to \infty$) Kay (1998), Galeazzi et al. (2013).

The probability of detecting a fault under $\mathcal{H}_1$, with probability P_D for a given threshold γ is given by

$$P_D = 1 - P(\gamma; \mathcal{H}_1, \nu, \lambda), \tag{35}$$

where $P(\cdot)$ is the cumulative distribution function of a given test statistics distribution.

4. PERFORMANCE ASSESSMENT

The GLRT performance is dependant on the trade-off between the desire for a high P_D, a low P_{FA}, GLRT window size N , and the time it takes to detect the occurrence of a fault.

The test statistics, from r_1 denoted $T_{r_1}(\mathbf{x})$, approximately follow a chi-squared ($\mathcal{X}_\nu^2$) distribution under $\mathcal{H}_0$ and a non-central $\mathcal{X}_\nu'^2(\lambda)$ under $\mathcal{H}_1$, with ν and λ serving as degree-of-freedom and non-centrality parameters, respectively. For window sizes $N = 1000, 2000$, corresponding to 10 and 20 seconds, a visual representation can be found in Figure 6, which also includes thresholds for $P_{FA} = 10^{-6}$. Here it should be mentioned that parameters of the $\mathcal{X}_\nu^2$, used to fit the data, were estimated utilising MLE.

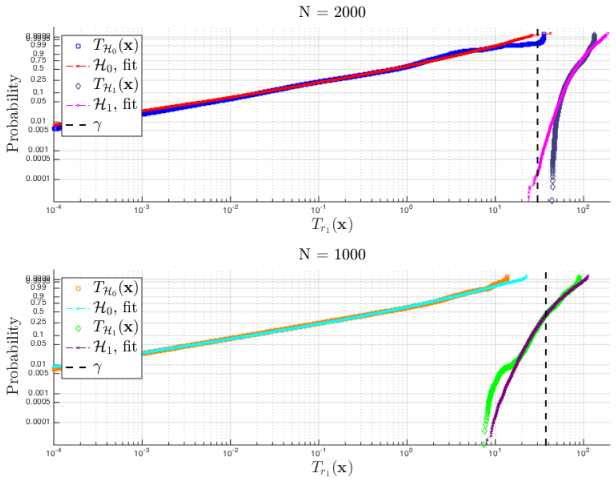

Fig. 6. Probability plot of $T(\mathbf{x})$, for r_1, under $\mathcal{H}_0$ and $\mathcal{H}_1$ for window length $N = 1000$ and $N = 2000$.

For r_2, the test statistics, denoted $T_{r_2}(\mathbf{x})$, display the same distribution characteristics as $T_{r_1}(\mathbf{x})$, i.e. $T_{r_2}(\mathbf{x})$ approximately follow a $\mathcal{X}_\nu^2$ distribution under $\mathcal{H}_0$ and a $\mathcal{X}_\nu'^2(\lambda)$ under $\mathcal{H}_1$. Choosing window sizes $N = 500, 1000$ the probability characteristics of $T_{r_2}(\mathbf{x})$ are displayed in Figure 7. The thresholds seen in the figure are for $P_{FA} = 10^{-6}$. The performance of the GLRT, for both residuals, are found in Table 2.

Table 2. GLRT performance

	$T_{r_1}(\mathbf{x})$		$T_{r_2}(\mathbf{x})$	
N	1000	2000	500	1000
P_{FA}	10^{-6}	10^{-6}	10^{-6}	10^{-6}
P_D	58.89%	99.99%	56.97%	96.46%

Note that wind turbulence levels significantly influence the evolution of the residuals, i.e. increased turbulence will result in a decrease in P_D, but this is easily accommodated by increasing the window size N. It is, however, the accelerometer measurement noise that is the primary contaminant. Consequently a white noise model could have

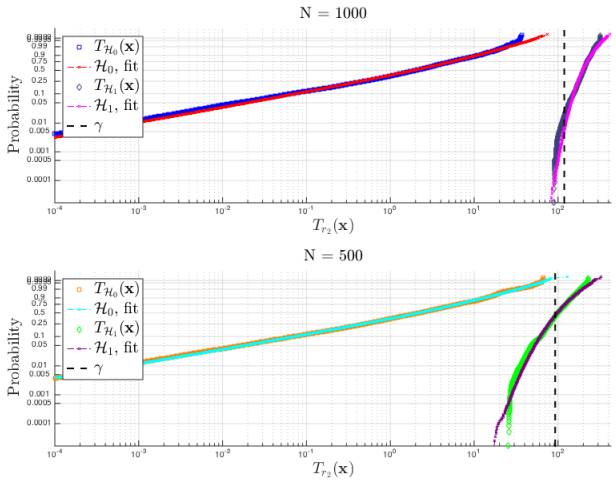

Fig. 7. Probability plot of $T(\mathbf{x})$, for r_2, under $\mathcal{H}_0$ and $\mathcal{H}_1$ for window length $N = 500$ and $N = 1000$.

limitations, as accelerometer noise might include issues such as bias, drift, vibrations, etc. that are correlated. Correlated noise can be addressed by pre-whitening. The issue of correlated noise and solutions is a subject deemed outside the scope of the work presented here.

5. CONCLUSION

The work presented in this paper proposes a Neyman Pearson based statistical change detection approach, for the identification of structural changes of fixed wing UAV airfoils. The solution employs structural analysis to identify residuals, which are processed by a generalised likelihood ratio test, utilised for hypotheses tests on potential changes and severity assessments, supplying estimates of the magnitude of change.

Simulations were conducted that show the expected performance under both nominal and icing influenced conditions. The proposed fault diagnosis solution ensures a high level of fault detection in spite of turbulent winds, measurement noise and model uncertainties. Thresholds were obtained ensuring a low probability of false alarms and achieving a high probability of detection. The detection was analysed using simulation generated data where a fault was imposed on the system.

REFERENCES

Bateman, F., Noura, H., and Ouladsine, M. (2011). Fault diagnosis and fault-tolerant control strategy for the aerosonde uav. *Aerospace and Electronic Systems, IEEE Transactions on*, 47(3), 2119–2137.

Beard, R.W. and McLain, T.W. (2012). *Small Unmanned Aircraft - Theory and Practice*. Princeton University Press.

Blanke, M. and Hansen, S. (2013). Towards self-tuning residual generators for uav control surface fault diagnosis. In *Control and Fault-Tolerant Systems (SysTol), 2013 Conference on*, 37–42.

Blanke, M., Kinnaert, M., Lunze, J., and Staroswiecki, M. (2006). *Diagnosis and Fault-Tolerant Control*. Springer Berlin Heidelberg.

Blanke, M. and Lorentzen, T. (2006). Satool - a software tool for structural analysis of complex automation systems. In *Proceedings of the 6. IFAC Symposium on Fault Detection, Supervision and Safety of Technical Processes*, 673–678. Elsevier Science.

Cristafaro, A. and Johansen, T.A. (2015). An unknown input observer approach to icing detection for unmanned aerial vehicles. In *American Control Conference*.

Cristafaro, A., Johansen, T.A., and Aguiar, A.P. (2015). Icing detection and identification for unmanned aerial vehicles: Multiple model adaptive estimation. In *European Control Conference*.

Ducard, G. (2009). *Fault-tolerant Flight Control and Guidance Systems*. Springer London.

Ducard, G. and Geering, H.P. (2008). Efficient nonlinear actuator fault detection and isolation system for unmanned aerial vehicles. *Journal of Guidance, Control, and Dynamics*, (1), 225–237.

Fravolini, M.L., Brunori, V., Campa, G., Napolitano, M.R., and La Cava, M. (2009). Structural analysis approach for the generation of structured residuals for aircraft fdi. *Aerospace and Electronic Systems, IEEE Transactions on*, 45(4), 1466–1482.

Galeazzi, R., Blanke, M., and Poulsen, N. (2013). Early detection of parametric roll resonance on container ships. *Control Systems Technology, IEEE Transactions on*, 21(2), 489–503.

Hansen, S. and Blanke, M. (2013). Diagnosis of airspeed measurement faults for unmanned aerial vehicles. *IEEE Transactions of Aerospace and Electronic Systems*.

Johansen, T.A., Cristafaro, A., Sørensen, K.L., Hansen, J.M., and Fossen, T.I. (2015). On estimation of wind velocity, angle-of-attack and sideslip angle of small uavs using standard sensors. In *International Conference on Unmanned Aircraft Systems*.

Kay, S.M. (1998). *Fundamentals of Statistical Signal Processing: Detection theory*. Prentice Hall Signal Processing Series. Prentice-Hall PTR.

Langelaan, J.W., Alley, N., and Neidhoefer, J. (2011). Wind field estimation for small unmanned aerial vehicles. *Journal of Guidance, Control, and Dynamics*, 34(4), 1016–1030.

Long, H. and Song, S. (2009). Method of estimating angle-of-attack and sideslip angel based on data fusion. In *Intelligent Computation Technology and Automation, 2009. ICICTA '09. Second International Conference on*, volume 1, 641–644. doi:10.1109/ICICTA.2009.160.

Lynch, F.T. and Khodadoust, A. (2001). Effects of ice accretions on aircraft aerodynamics. *Progress in Aerospace Sciences*, 37(8), 669 – 767.

Stevens, B. and Lewis, F. (2003). *Aircraft Control and Simulation*. Wiley.

Tousi, M. and Khorasani, K. (2009). Fault diagnosis and recovery from structural failures (icing) in unmanned aerial vehicles. In *Systems Conference, 2009 3rd Annual IEEE*, 302–307.

Tousi, M. and Khorasani, K. (2011). Robust observer-based fault diagnosis for an unmanned aerial vehicle. In *Systems Conference (SysCon), 2011 IEEE International*, 428–434.